Redox Biology 8 (2016) 149–159

Contents lists available at ScienceDirect

Redox Biology

journal homepage: www.elsevier.com/locate/redox

Research Paper

Prominent role of exopeptidase DPP III in estrogen-mediated protection against hyperoxia *in vivo*

Sandra Sobočanec [a,*,1], Vedrana Filić [b,1], Mihaela Matovina [c], Dragomira Majhen [b], Željka Mačak Šafranko [a], Marijana Popović Hadžija [a], Željka Krsnik [d], Andrea Gudan Kurilj [e], Ana Šarić [a], Marija Abramić [c], Tihomir Balog [a]

[a] Division of Molecular Medicine, Ruđer Bošković Institute, Zagreb, Croatia
[b] Division of Molecular Biology, Ruđer Bošković Institute, Zagreb, Croatia
[c] Division of Organic Chemistry and Biochemistry, Ruđer Bošković Institute, Zagreb, Croatia
[d] Croatian Institute for Brain Research, University of Zagreb School of Medicine, Zagreb, Croatia
[e] Department of Veterinary Pathology, Faculty of Veterinary Medicine, University of Zagreb, Zagreb, Croatia

ARTICLE INFO

Article history:
Received 6 December 2015
Received in revised form
5 January 2016
Accepted 8 January 2016
Available online 11 January 2016

Keywords:
Hyperoxia
DPP III
Estradiol
Mice
Oxidative stress
Nrf-2
Sirt-1
Ho-1
Ppar-γ

ABSTRACT

A number of age-related diseases have a low incidence in females, which is attributed to a protective effect of sex hormones. For instance, the female sex hormone estrogen (E_2) has a well established cytoprotective effect against oxidative stress, which strongly contributes to ageing. However, the mechanism by which E_2 exerts its protective activity remains elusive.

In this study we address the question whether the E_2-induced protective effect against hyperoxia is mediated by the Nrf-2/Keap-1 signaling pathway. In particular, we investigate the E_2-induced expression and cellular distribution of DPP III monozinc exopeptidase, a member of the Nrf-2/Keap-1 pathway, upon hyperoxia treatment.

We find that DPP III accumulates in the nucleus in response to hyperoxia. Further, we show that combined induction of hyperoxia and E_2 administration have an additive effect on the nuclear accumulation of DPP III. The level of nuclear accumulation of DPP III is comparable to nuclear accumulation of Nrf-2 in healthy female mice exposed to hyperoxia. In ovariectomized females exposed to hyperoxia, supplementation of E_2 induced upregulation of DPP III, Ho-1, Sirt-1 and downregulation of Ppar-γ. While other cytoprotective mechanisms cannot be excluded, these findings demonstrate a prominent role of DPP III, along with Sirt-1, in the E_2-mediated protection against hyperoxia.

1. Introduction

The excessive production of various types of reactive oxygen/nitrogen species (ROS/RNS) can directly damage cellular macromolecules and thus lead to cell death, especially under prolonged oxygen supplementation, i.e. chronic hyperoxic exposure [1]. The major antioxidant enzymes prevent the formation of toxic ROS/RNS, and oxidative stress ensues when the formation of these species exceeds the capacity of the antioxidative mechanisms to neutralize them. Resistance to hyperoxia can be used as an indicator of the longevity potential of an organism, since hyperoxia has been shown to reduce the lifespan and to induce a similar level of oxidative damage and similar gene expression patterns as aging [2]. In accord with these findings, cellular resistance to oxidative stress has been positively correlated with mammalian longevity [3].

17-β estradiol (E_2), a female sex hormone, has a wide variety of physiological effects on a number of cell types. E_2 has well-established cytoprotective effect during oxidative stress and its depletion contributes to pathogenesis of several age-related diseases [4]. Previously, we have shown that females had better survival, increased resistance and more efficient defense systems against hyperoxia compared to males, and that their resistance to hyperoxia might be a consequence of the beneficial effect of ovarian hormones [5]. We have also recently shown in vivo that E_2 upregulates the level of dipeptidyl peptidase III (DPP III), a monozinc exopeptidase that hydrolyzes dipeptides from the N-terminus of

Abbreviations: E2, 17-β estradiol; DPP III, dipeptidyl peptidase III; Nrf-2, NF-E2-related factor 2 Keap-1, Kelch-like ECH-associated protein 1; Ho-1, heme oxygenase 1; Sirt-1, sirtuin 1; Ppar-γ, peroxisome proliferator-activated receptor gamma; ARE, antioxidant response element

* Corresponding author.
E-mail address: ssoboc@irb.hr (S. Sobočanec).
[1] These authors have equally contributed to this work.

http://dx.doi.org/10.1016/j.redox.2016.01.003
2213-2317/

its substrates consisting of three or more amino acids [6]. DPP III is involved in the endogenous defense against oxidative stress, being a part of Nrf-2/Keap-1 signaling pathway [7,8]. In mammalian tissues, DPP III is ubiquitously distributed and thought to contribute to the final steps of normal intracellular protein catabolism [9]. NF-E2-related factor 2 (Nrf-2) is a transcription factor that induces gene expression of antioxidant enzymes and many other cytoprotective enzymes through binding to antioxidant response elements (ARE) [10]. Under physiological conditions, Nrf-2 is inhibited via binding to Kelch-like ECH-associated protein 1 (Keap-1) [11]. Upon a stressful insult, Nrf-2 dissociates from Keap-1, translocates into the nucleus and activates ARE-dependent gene expression, thereby reducing the injury to cells [12]. Ppar-γ is a cytoprotective protein controlled by Nrf-2/Keap-1 [13], and involved in lipid and glucose metabolism, insulin resistance [14] and antiinflammatory response [15]. In the liver, Ppar-γ is expressed at a low basal level, but is upregulated in murine models of obesity and type two diabetes [16]. Sirtuin (Sirt-1) is a conserved NAD-dependent histone deacetylase that has been linked to longevity and energy homeostasis [17], and shown to be important in suppression of common age-related diseases [18]. Moreover, Sirt-1 mediates the calorie restriction (CR)-induced prolongation of lifespan by suppression of Ppar-γ [19].

The main goal of the present study is to determine whether the protective effect of E_2 against hyperoxia relies on the Nrf-2/Keap-1 signaling pathway. We therefore investigate the effect of hyperoxia on the DPP III expression and cellular localization, and their dependence on E_2 supplementation. We further characterize the hyperoxia-induced behavior of enzymes involved in cellular response towards oxidative stress, such as Sirt-1, Ppar-γ and Ho-1. Our results suggest that the Nrf-2/Keap-1 pathway, which involves DPP III, mediates the cytoprotective effect of E_2.

2. Material and methods

2.1. Animals and hyperoxia exposure

All experiments were performed in accordance with the current legislation of the Republic of Croatia and with the guidelines of European Community Council Directive of November 24, 1986 (86/609/EEC). Female CBA/H mice aged 4 months from breeding colony of the Ruđer Bošković Institute (Zagreb, Croatia) were used for all experiments. The animals were maintained under the following laboratory conditions: three to a cage; light on from 06:00 to 18:00; 22 ± 2 °C room temperature; access to food pellets, and tap water ad libitum. Hyperoxic oxygen conditions were carried out by flushing the chamber (Đuro Đaković, Slavonski Brod, Croatia) with pure oxygen (25 L/min for 10 minutes) to replace air. After that mice were placed in the chamber for 46 h, and allowed to breathe pure oxygen. Normoxic O_2 conditions serving as a control were obtained by keeping mice in the same chamber, but under ambient air. Mice were assigned randomly into following groups: normoxia-treated sham-operated females (sham), hyperoxia-treated sham-operated females (hsham), hyperoxia-treated ovariectomized females (hovx), and hyperoxia-treated ovariectomized females with E_2 (hovxe).

2.2. Ovariectomy procedure and E_2 administration

Ovariectomy and sham surgery were performed under ketamine/xilazyne anesthesia. Since low levels of E_2 are normally detected in ovariectomized females due to other endogenous E_2 sources [20], plasma E_2 levels were not used as indicator of efficiency of ovariectomy. Instead, the success of ovariectomy was assessed by analyzing vaginal smear during 5 consecutive days after the surgery (data not shown). In our preliminary experiments we established that anestrus phase seen on vaginal smear is reflected by uterus atrophy as evaluated post-mortem. To allow mice to recover after the surgery, measurements started seven days after the surgery. For E_2 administration, a pellet containing E_2 (50 μg, Innovative Research of America, Sarasota, FL) was placed into the interscapular subcutaneous space releasing a constant dose of 830 ng daily. After 37 days post-surgery, animals were subjected to experimental procedures.

2.3. Body weight measurement

Body weight gain was used as a marker of successful ovariectomy, since ovariectomy-induced body weight gain is the established phenomenon. All animals were weighted prior to any experiment to ensure there are no significant differences between groups. At 37th day post-surgery, animals were weighted again and subjected to experimental procedures.

2.4. Oxidative damage parameters

Lipid peroxidation was assessed by measuring the formation of thiobarbituric reactive substances (TBARS) at 532 nm, according to [20]. The results were expressed as nmol TBARS/mg of protein in liver supernatant according to a standard curve which was prepared with serial dilutions of 1,1,3,3-tetramethoxypropane. Comet assay was carried out under alkaline conditions, as described in [21]. One hundred randomly selected cells per sample were analyzed by an automatic digital analysis system Comet assay IV, at 250 × magnification (Perspective Instruments Ltd., Suffolk, Halstead, UK). To quantify DNA damage, the tail moment (tail length × tail % DNA/100) was evaluated. One hundred comets were measured on 3 slides per each group. Since the data of the comet assay measurements are usually more or less dispersed, the statistical analysis and graphical presentation of the data were performed using the adequate statistical method that takes into account the non-Gaussian distribution of the data.

2.5. Determination of glutathione level

The levels of oxidized (GSSG) and reduced glutathione (GSH) in liver supernatants were measured using assay kit for detection of total, reduced and oxidized glutathione (ADI-900-160, Enzo Life Sciences, NY, USA), according to the manufacturer's instructions. Briefly, livers were homogenized in 5% meta-phosphoric acid, following centrifugation at 13,000*g* for 15 min. The resulting supernatant was subjected to determination of total GSH, while for GSSG determination, the supernatant was incubated with 2M 4-vinylpyridine for one hour at room temperature.

2.6. RNA isolation and real-time PCR analysis

Total RNA was extracted from individual mouse liver ($n=3$ per each group) using TRIzol reagent (Invitrogen, Carlsbad, CA, USA) according to the manufacturer's instructions. To quantify relative gene expression of dpp III, sirt-1, ppar-γ and ho-1, reverse transcription and real-time PCR analysis were done as described previously [22]. Data were analyzed using the $2^{-\Delta\Delta Ct}$ method and presented as the fold-change in dpp III, sirt-1, ppar-γ and ho-1 gene expression normalized to endogenous reference gene (β-actin) and relative to the untreated control. Assays used in this study are listed in Supplemental file, Table S1. All reactions were carried out in triplicate.

2.7. SDS-PAGE and western blot analysis

Liver was homogenized with RIPA buffer supplemented with proteinase inhibitors (10% w/v) using an ice-jacketed Potter-Elvehjem homogenizer (1300 rpm). After sonication (3 × 30 s), whole liver homogenates were centrifuged at 16,000*g* for 20 min at 4 °C. The resulting supernatant was collected and total cellular proteins (75 μg per lane) were resolved by SDS-PAGE and transferred onto a PVDF membranes (Bio-Rad, Hercules, CA). Membranes were blocked in 5% nonfat dry milk in TN buffer (50 mM TRIS, 150 mM NaCl, pH 7.4) overnight and after that incubated with primary polyclonal rabbit antibody against DPP III (antiserum diluted 1:200 and incubated for 3 h at room temperature), Sirt-1 (Santa Cruz Biotechnology Inc, TX, USA) diluted 1:200 and incubated overnight at +4 °C, Ppar-γ (Santa Cruz Biotechnology Inc, TX, USA) diluted 1:200 and incubated overnight at +4 °C, and Ho-1 (Abcam Inc., Cambridge, UK) diluted 1:1000 and incubated for 3 h at room temperature. All incubations were followed by incubation with donkey anti-rabbit IgG, horseradish peroxidase-conjugated, secondary antibody diluted 1:2000 (Amersham Biosciences Inc., USA). Equality of loading was confirmed using AmidoBlack (Sigma Aldrich, St.Louis, USA), which was also used for normalization of the bands. The chemiluminescence signals were detected and analyzed with the Alliance 4.7 Imaging System (UVITEC, Cambridge, UK). The experiments were repeated at least three times and representative blots are presented.

2.8. Immunohistochemistry and fluorescence intensity quantification

After perfusion, liver tissue was fixed by immersion in 4% paraformaldehyde in 0.1 M PBS (pH 7.4), blocks were embedded in paraffin, sectioned at 12 μm and deparaffinized through a graded series of xylol and alcohols. Sections were then processed according to [23], with small modification of the protocol. After incubation in blocking solution (BS, 5% BSA in 0.1 M PBS and 0.5% Triton X-100) to prevent nonspecific background staining, tissue sections were incubated overnight at 4 °C with rabbit anti-DPP III polyclonal antibody, diluted 1:200 (Abcam Inc. Cambridge, UK) then rinsed and incubated at room temperature with fluorescein isothiocyanate (FITC) conjugated anti-rabbit IgG antibody (Vector Laboratories Inc., Peterborough, UK), diluted 1:100. Followed by rinsing and incubation with 1 μg/ml DAPI (Sigma Aldrich, St. Louis, USA) in 0.1 M PBS, sections were coverslipped with Aqueous Mounting Medium (DAKO, Carpinteria, CA, USA). Negative controls were included in all immunofluorescence experiments by replacing the primary antibody with BS and no signal was detected. Confocal fluorescence microscopy has been performed on the laser scanning microscope Leica TCS SP8 X (Leica Microsystems, Wetzlar, Germany). Images were acquired by sequential scanning with the excitation at 405 nm for DAPI, and 490 nm for FITC. Detection ranges were 412–480 nm for DAPI, and 500–585 nm for FITC. Intensities in the FITC channel were quantified using Leica Application Suite LAS AF (version 3.2.1.9702). Ratio between average fluorescence intensities in the nucleus and the cytoplasm, I(nucleus)/I(cytoplasm), was determined for at least 60 cells per sample.

2.9. Nuclear extract preparation and western blot analysis

In order to confirm the accumulation of DPP III in nucleus upon treatments, as revealed by confocal microscopy, we have isolated nuclear fractions as previously described [24], and subjected all groups to immunoblot analysis using anti-DPP III polyclonal antibody (custom made by Abcore, USA). Also, we have investigated the nuclear accumulation of both Nrf-2 and Keap-1 in the same experimental groups. Briefly, the liver tissue was homogenized in hypotonic buffer containing 10 mM HEPES, pH 7.9, 1 mM $MgCl_2$, 0.5 mM EDTA, 1 mM dithiothreitol (DTT), 1% Triton X-100 and 0.5 mM phenylmethylsulfonylfluoride. The lysates were sonicated (3 × 30 s), incubated for 20 min at +4 °C and centrifuged at 2000*g* for 5 min at +4 °C. The resulting supernatant was discarded, while pellets containing crude nuclei were resuspended in 150 μl of extraction buffer containing 20 mM HEPES, pH 7.9, 300 mM NaCl, 0.2 mM EDTA, 2 mM dithiothreitol, and 0.5 mM phenylmethylsulfonylfluoride and incubated for 30 min at +4 °C. The samples were centrifuged at 15,000*g* for 20 min to obtain supernatants containing nuclear fractions. The purity of the nuclear fractions was confirmed by immunoblot analysis using a primary rabbit polyclonal antibody against histone H3 diluted 1:2000 (Abcam Inc., Cambridge, UK). Membranes were blocked in 5% nonfat dry milk in TN buffer (50 mM Tris–HCl, 150 mM NaCl, pH 7.4) for one hour at 37 °C, followed by overnight incubation at +4 °C with anti-DPP III polyclonal antibody (custom made by Abcore, USA), anti-Nrf2 (Abcam Inc., Cambridge, UK), diluted 1:200 and anti-Keap-1 (Abcam Inc., Cambridge, UK), diluted 1:500. The membranes were subsequently incubated with horseradish peroxidase-conjugated donkey anti-rabbit IgG secondary antibody diluted 1:2000 (Amersham Biosciences Inc., Piscataway, NJ, USA) for one hour at room temperature. Amido Black (Sigma-Aldrich, St. Louis, MO, USA) was used for the determination of equal sample loading. The experiments were repeated three times and the representative immunoblots are shown.

2.10. DPP III activity assay

Cytosolic DPP III activity in liver homogenates from all groups was determined by standard assay with Arg-Arg-2-naphthylamide (Arg_2-2NA) (Bachem, Bubendorf, Switzerland) as the substrate [9]. The reaction mixture (total volume of 1 ml) containing 50 mM Tris–HCl, pH 8.6, 50 μM $CoCl_2$, appropriate amount of liver cytosols (approximately 20–40 μg of proteins per ml of reaction mixture), and 30 μM aminopeptidase inhibitor bestatin (Sigma-Aldrich, St. Louis, MO, USA) was preincubated for 20 min at room temperature, followed by 2 min at 37 °C. The reaction is initiated by the addition of 0.04 mM Arg_2-2NA, and the reaction mixture was incubated at 37 °C for 15 min. The reaction was stopped by the addition of 0.2 ml of 10% Tween 20 in 2 M acetate buffer (pH 4.2) containing 1.5 mg/ml of stabilized diazonium salt Fast Blue B (Sigma-Aldrich, St. Louis, MO, USA) for coupling of released 2-naphthylamine. The absorbance was measured spectrophotometrically at 530 nm. One unit of enzyme activity (U) was defined as the amount of enzyme which converts 1 μmol of substrate per minute under the assay conditions. Specific activity of DPP III was expressed in milliunits per mg of the protein.

2.11. Histopathological analysis

Histological analysis of liver tissue from all experimental groups was performed in order to determine the hepatic damage caused by hyperoxia. Slides were prepared from formalin-fixed paraffin-embedded liver stained with haematoxylin and eosin. All immunohistochemical analyses were done by a pathologist oblivious of the study group design.

2.12. Protein concentration

Protein concentration in all samples was determined using BCA protein assay (Thermo Scientific, Rockford, USA).

2.13. Statistical analysis

Statistical analyses of data were performed using R v2.15.3 (CRAN, http://cran.r-project.org) and RStudio for Windows, v 0.97

(http://www.rstudio.com/). Before all analyses, samples were tested for normality of distribution using Shapiro–Wilk test. If data followed non-Gaussian distribution, nonparametric analyses were performed: Kruskal–Wallis non-parametric ANOVA, followed by Wilcoxon signed-rank test for testing differences between two related groups. Statistical analysis of comet test results was performed on logarithmically transformed data. In case of normal distributions, parametric tests were performed: one-way ANOVA, followed by Tukey's post-hoc tests for multiple comparisons of the samples. For all experiments the individual samples were used and processed separately for each procedure. No pooled samples were used throughout the study.

3. Results

3.1. The increase in body weight induced by ovariectomy and prevention by E2

We have used the body weight gain as a marker of successful ovariectomy, since it is well documented that ovarian hormone depletion is in association with increased body weight [25]. We have shown that ovariectomy induced significant increase in body weight ten days after the surgery, and this increase persisted throughout duration of the experiment. The E_2 administration prevented the body weight gain induced by ovariectomy, while exposure to hyperoxia had no effect on body weight gain. The results of body weights are presented as mean ± S.D., and shown in Supplemental file, Table S2. The observed significant differences in total body weight between groups are shown in Supplemental file, Table S3. The number of samples was: $n=5$ (sham), $n=7$ (hsham), $n=8$ (hovx) and $n=7$ (hvoxe).

3.2. The effect of E_2 on hepatic lipid peroxidation (LPO) and DNA damage in the liver of hyperoxia-treated female CBA/H mice

Hepatic lipid oxidative damage was evaluated by measuring TBARS levels in the supernatant of liver homogenate of all experimental groups. The number of samples was: $n=5$ (sham), $n=7$ (hsham), $n=8$ (hovx) and $n=7$ (hvoxe). Compared to sham-operated normoxic females, in sham-operated females under hyperoxia TBARS did not accumulate. However, a significant increase in TBARS levels was observed in ovariectomized group under hyperoxic conditions, compared to all other groups (Fig. 1A; $^{a}p=0.003$ sham vs. hovx; $^{b}p=0.004$ hsham vs. hovx; $^{c}p=0.002$ hovxe vs. hovx). E_2 abolished this effect by lowering TBARS level back to values found in sham group of mice. The effect of hyperoxia on DNA damage was assessed by the single-cell gel electrophoresis (comet assay) and is shown in Fig. 1B. One-hundred comets were measured on 3 slides per each group. The observed significant differences in DNA damage between groups are presented in Supplemental file, Table S4. (Kruskal–Wallis chi-squared=31.5192, df=4, $p<0.001$). Interestingly, hyperoxia markedly lowered DNA damage in all groups, especially in hsham mice, in comparison to control sham group. When we compared hsham group with ovariectomized females under hyperoxia, we have observed marked increase in DNA damage in hovx females which could only partially be lowered back to levels in hsham group by the administration of E_2.

3.3. Assessment of the oxidative stress in liver of hyperoxia-treated female CBA/H mice by determining the levels of oxidized and reduced glutathione

The ratio between GSSG and total glutathione concentrations is often used to assess the level of oxidative stress in the cell. We have determined GSSG and GSH cellular concentrations in order to see whether hyperoxia, alone or in combination with manipulation of E_2, influenced this major component of the cellular antioxidant machinery (Fig. 2). Our results show that in mice subjected to hyperoxia, GSSG/total GSH ratio was slightly increased ($^{a}p<0.05$), while in mice subjected to hyperoxia and depleted of E_2, the ratio increased more than 70%, compared to both normoxic group ($^{b}p<0.001$) and hsham group ($^{d}p<0.001$), clearly showing the presence of oxidative stress in these samples. Although E_2 administration induced decrease in GSSG level by almost 40% compared to hovx group ($^{e}p<0.001$), the level of oxidized form in

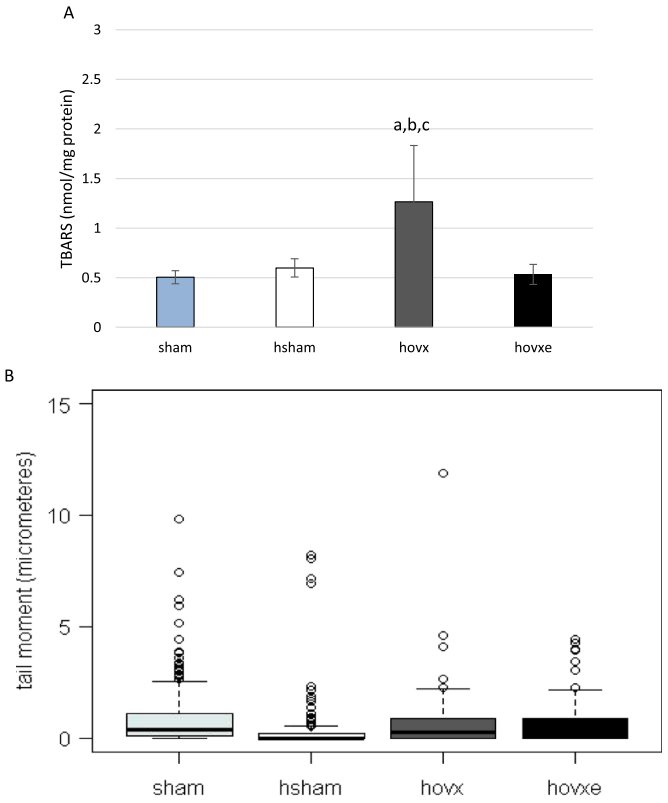

Fig. 1. TBARS levels in liver of female CBA/H mice subjected to hyperoxia. Small letters designate p values: ($^{a}p=0.003$ sham vs. hovx; $^{b}p=0.004$ hsham vs. hovx; $^{c}p=0.002$ hovx vs. hovxe). Results are expressed as mean ± S.D. The number of mice per each group was: $n=5$ (sham), $n=7$ (hsham), $n=8$ (hovx) and $n=7$ (hvoxe) (A). Comet assay as a measure of DNA damage expressed as tail moment in female CBA/H mice subjected to hyperoxia (B). The probability in the Mann–Whitney U test for differences between groups is presented in Table S4. The number of mice per each group: $n=5$ (sham), $n=7$ (hsham), $n=8$ (hovx) and $n=7$ (hvoxe).

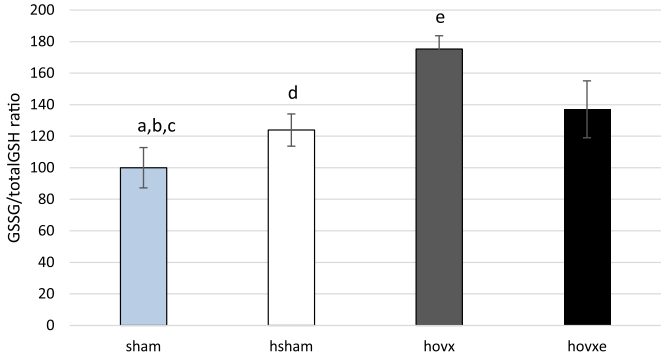

Fig. 2. GSSG/total GSH ratio in livers of hyperoxia-treated female CBA/H mice. Small letters denote p values. $^{a}p<0.05$, sham vs. hsham; $^{b}p<0.001$, sham vs. hovx; $^{c}p<0.01$, sham vs. hovxe; $^{d}p<0.001$, hsham vs. hovx; $^{e}p<0.001$ hovx vs. hovxe. Results are presented as percentage of mean ± S.D. and normalized to sham group. The number of samples was $n=6$ per each group.

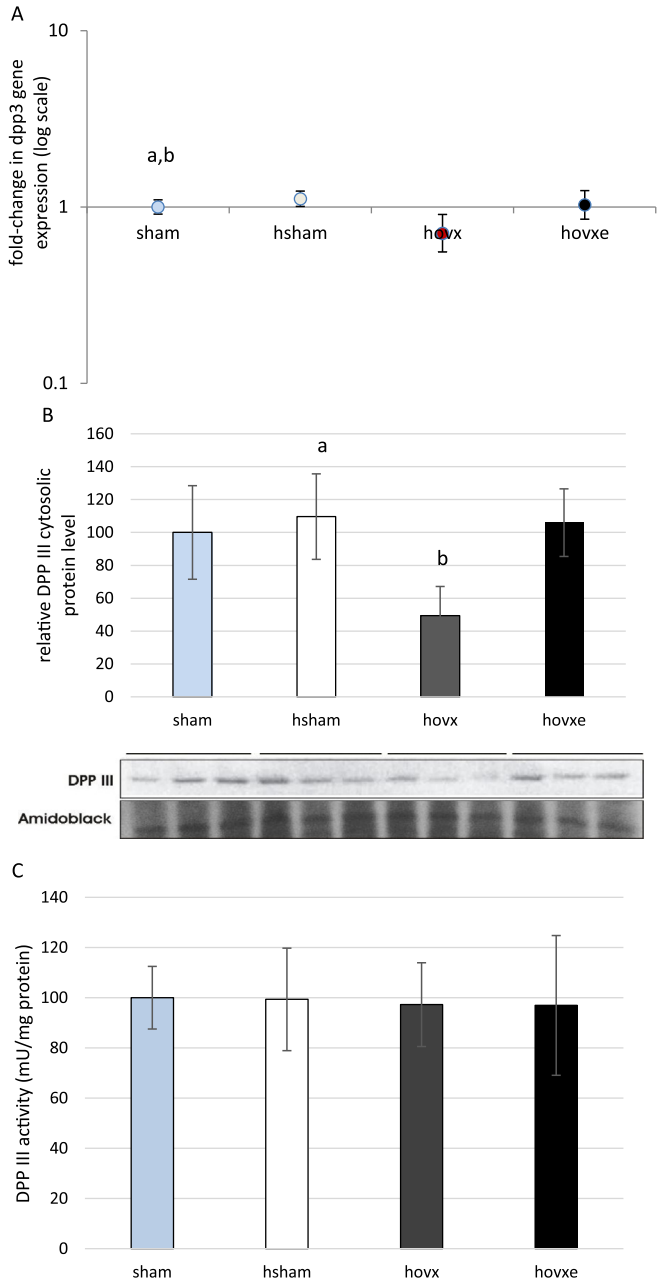

Fig. 3. Real-time PCR analysis of dpp III gene expression in the liver of female CBA/H mice subjected to hyperoxia. The fold change in gene expression was calculated using the $2^{-\Delta\Delta CT}$ method and β-actin as the endogenous control. The results are presented as fold-change ± S.E. and normalized to sham group. The number of samples was $n=3$ per each group. Small letters denote p values. $p<0.001$, sham vs. hsham; $^{b}p=0.033$, hsham vs. hovx (A). Western blot analysis of DPP III protein expression in the liver of female CBA/H mice subjected to hyperoxia. Results are presented as mean ± S.D. Amidoblack was used as a loading control. The number of samples was $n=3$ per each group. $^{a}p=0.029$, hsham vs. hovx; $^{b}p=0.022$, hovx vs. hovxe (3B). DPP III activity in liver cytosol of sham, hsham, hovx and hovxe CBA/H females. Results are expressed as mean ± S.D. and normalized to sham group. The number of samples was $n=6$ per each group (3C).

E_2-administered mice was still 37% higher than in normoxic group ($^{c}p<0.01$). The number of samples was $n=6$ per each group.

3.4. The effect of E_2 on gene expression, protein level and activity of DPP III

In order to determine if E_2 exerts any effect on DPP III in hyperoxia, real-time PCR (Fig. 3A), western blot analysis (Fig. 3B) and the measurement of DPP III activity (Fig. 3C) were performed in liver cytosol of all samples. For the analysis of dpp III gene expression and the analysis of Dpp III protein level, the number of samples was $n=3$ per each group. For the measurement of Dpp III activity, the number of samples was $n=6$ per each group. Our results show the increased dpp III gene expression in hsham group, compared to sham group ($^{a}p<0.001$, sham vs. hsham), but with no significant increase in protein level. However, under hyperoxic conditions ovariectomy induced markedly decreased mRNA level ($^{b}p=0.033$, hsham vs. hovx) which was followed by decreased DPP III protein content in the cytosol ($p=0.029$, hovx vs. hsham). E_2 administration was able to revert cytosolic DPP III protein level back to normoxic levels, thus being significantly increased compared to hovx group ($p=0.022$, hovx vs. hovxe). However, the activity of DPP III remained constant in all groups of animals, despite any treatment or combination of treatments.

3.5. The effect of E_2 on nuclear localization of DPP III

Next, we were interested in the cellular localization of DPP III inside murine hepatocytes and whether it is influenced by acute oxidative stress alone, or in combination with E_2 manipulation. We have employed confocal microscopy with DPP III immunolabeling and observed strong cytosolic staining with only weak signal in the nuclei of sham-operated females under normoxic conditions (Fig. 4A). Interestingly, DPP III signal in the nucleus was significantly increased in all treated groups. Although hyperoxia increased nuclear staining of DPP III in both hsham (Fig. 4B) and hovx groups (Fig. 4C), the greatest increase in the nuclear signal intensity was observed in hovxe group. Namely, the E_2 administration to hovx females was associated with 25% increase of DPP III content in the nuclei compared to sham group (Fig. 4D). The number of samples was $n=2$ per each group.

Graphical display of the ratio between average fluorescence intensities in the nucleus and the cytoplasm is shown in Fig. 4E. The observed significant differences in signal intensities between groups are shown in Fig. 4F.

In order to validate results acquired by confocal microscopy, which showed significant protein accumulation in nucleus upon all treatments, we have immunoblotted nuclear fractions of liver cells of all experimental groups with anti-DPP III antibodies. Western blot analysis also showed DPP III accumulation in the nucleus in response to both hyperoxia and E_2 treatments. Although differences were on the border of statistical significance due to great variations between samples, the most intense signal was again observed in hyperoxia-exposed ovariectomized females treated with E_2, thus clearly indicating shift in DPP III localization toward nucleus ($^{a}p=0.042$, sham vs. hovxe) (Fig. 5A, B). The experiments were repeated three times and the representative immunoblot of one sample per group is presented.

3.6. The effect of E_2 on Nrf-2/Keap-1 protein level

Regarding the regulatory role of Nrf-2 protein in transcription of antioxidant and cytoprotective enzymes, we wanted to determine whether E_2 depletion under the acute oxidative stress is associated with the nuclear accumulation of Nrf-2. To address this question, we have performed western blot analyses for both Nrf-2 and Keap-1 proteins on nuclear fractions. The number of samples was $n=2$ per each group.

Nrf-2 showed almost 3-fold increase in nuclear accumulation in hsham ($^{a}p=0.008$, sham vs. hsham) and in hovx mice ($^{b}p=0.010$, sham vs. hovx) in comparison to sham group, where Nrf-2 was barely visible. Combined effect of hyperoxia and E_2 depletion with subsequent administration of E_2 lowered Nrf-2 nuclear level close to the margin of statistical significance, most

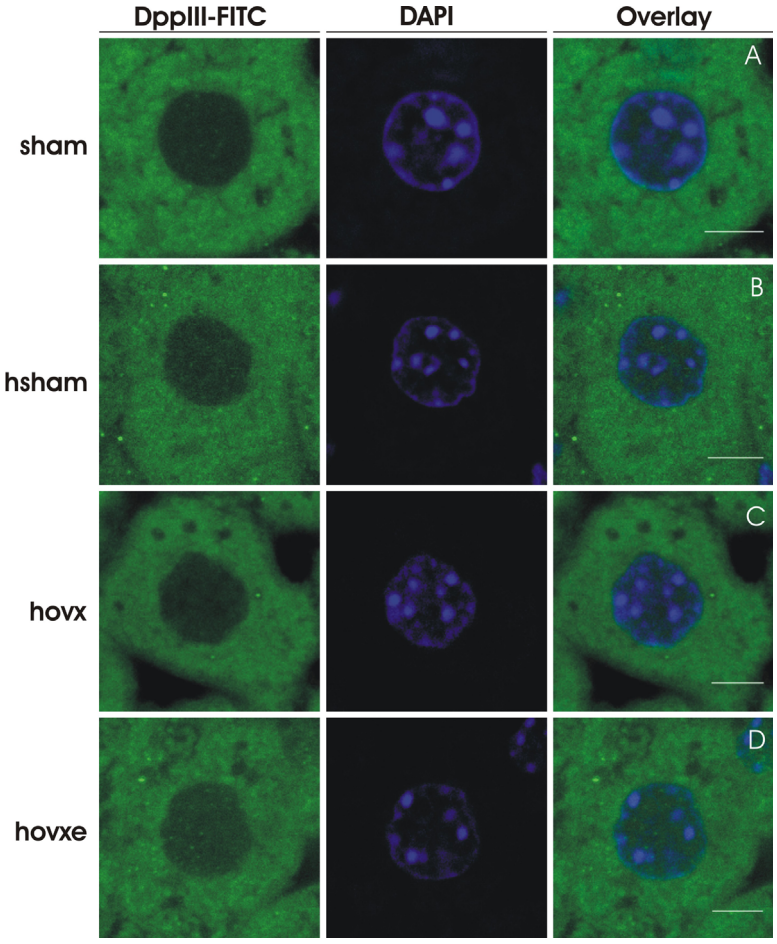

E

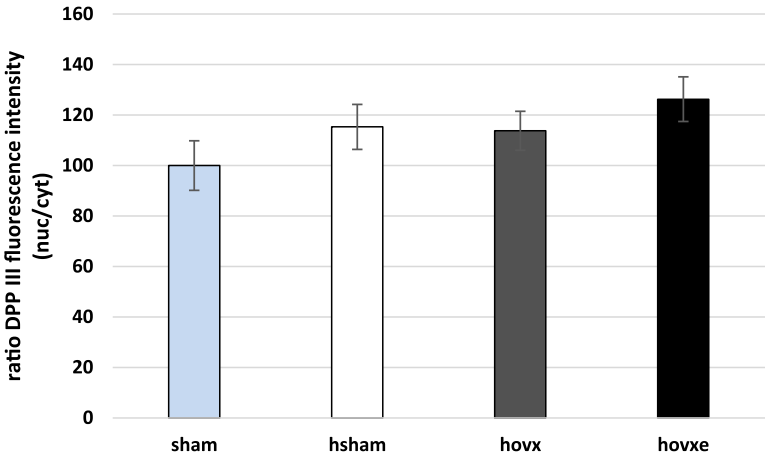

F

	sham	hsham	hovx	hovxe
sham	1	p<0.001	p<0.001	p<0.001
hsham	p<0.001	1	n.s.	p<0.001
hovx	p<0.001	n.s.	1	p<0.001
hovxe	p<0.001	p<0.001	p<0.001	1

Fig. 4. DPP III translocates from the cytosol into the nucleus in response to both hyperoxia and E_2 administration in hepatic tissue of female CBA/H mice. Representative confocal images, of both FITC (green) and DAPI (blue) channels, of each sample are shown. In sham-operated group of female CBA/H mice only very weak nuclear staining of DPP III can be observed (A); enhanced intensities of DPP III nuclear signal are found in the nucleus after hyperoxia (B), and after hyperoxia combined with ovariectomy (C); while the most intense nuclear signal was seen after combined treatments of hyperoxia and E_2 addition ($p=0.042$, sham vs. hovxe). (D). Graphical display of the ratio between average fluorescence intensities in the nucleus and the cytoplasm, normalized to the ratio of sham group. (E). Differences in signal intensities between test groups were further analyzed using post-hoc Wilcoxon signed-rank test (matrix of probabilities for the pairwise comparisons) (F). The number of samples was $n=2$ per each group. Results are expressed as mean $\pm$ S.D. and normalized to sham group. Bars represent 5 μm. (For interpretation of the references to color in this figure legend, the reader is referred to the web version of this article.)

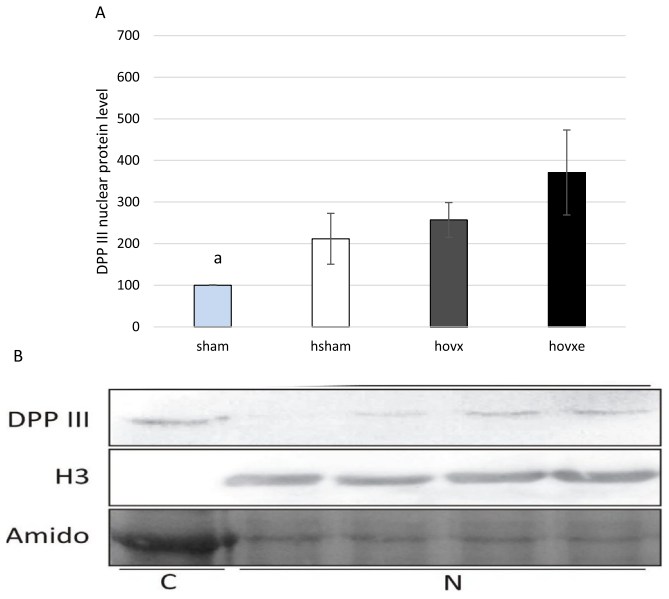

Fig. 5. Western blot analysis of DPP III protein level in the nucleus of sham, hsham, hovx, and hovxe groups of mice. Combined effect of hyperoxia and E_2 administration significantly increased nuclear DPP III level, compared to normoxic sham-operated group of mice ($^{a}p=0.042$, sham vs. hovxe) (A). Representative DPP III immunoblots of hepatic nuclear fractions. Histone H3 was used to assess the purity of nuclear fraction. Amidoblack was used as a loading control. The results are presented as mean ± S.D. and normalized to sham group. The experiments were repeated three times and the representative immunoblot of one sample per group is presented. Letters C and N designate cytosolic and nuclear fraction, respectively, while numbers denote sample groups as follows: 1-sham; 2-hsham; 3-hovx; 4-hovxe (B).

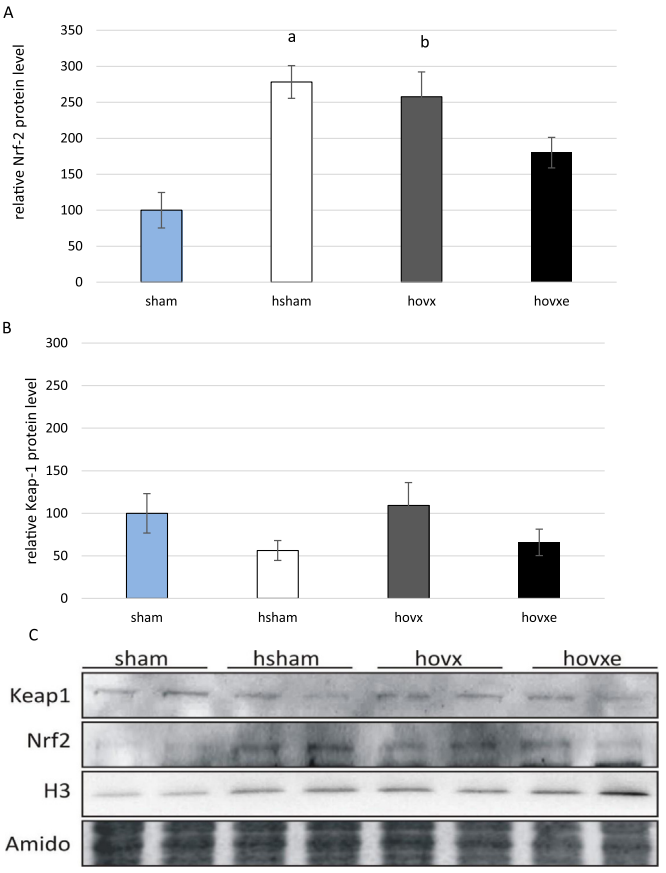

Fig. 6. Western blot analysis of Nrf-2 and Keap-1 protein levels in the nucleus of sham, hsham, hovx, and hovxe groups of mice. Nrf-2 level is significantly increased in the nucleus of mice treated with hyperoxia alone. Small letters denote p values. ($^{a}p=0.008$, sham vs. hsham mice), as well as in mice treated with the combination of hyperoxia and ovariectomy ($^{b}p=0.010$, sham vs. hovx) in comparison to normoxic group of animals (A). Nuclear accumulation of Keap-1 remained unchanged regardless of any treatment (B). Representative immunoblots of Nrf-2 and Keap-1 proteins in nuclear fractions of sham, hsham, hovx and hovxe group of mice are shown. Histone H3 was used to assess the purity of nuclear fraction. Amidoblack was used as a loading control. The results are presented as mean ± S.D. and normalized to sham group (C). The number of samples was $n=2$ per each group.

probably due to small sample size ($p=0.065$, hsham vs. hovxe) (Fig. 6A). The nuclear level of Keap-1 was relatively stable regardless of any treatment (Fig. 6B). Representative immunoblots of nuclear Nrf-2 and Keap-1 protein levels are shown in Fig. 6C.

3.7. The effect of E_2 on Sirt-1 and Ppar-γ expression level

Considering involvement of Sirt-1 and Ppar-γ in oxidative stress, we decided to investigate whether these proteins contribute to beneficial effect of E_2 in hyperoxic conditions. We have determined their gene expression and protein levels in all experimental groups and the number of samples was $n=3$ per group. Although we have not found statistically significant change in sirt-1 gene expression (Fig. 7A), we have noticed marked down-regulation of Sirt-1 protein in hovx group, compared to sham group ($^{d}p=0.035$, sham vs. hovx). E_2 administration induced Sirt-1 protein upregulation to levels even higher than in sham group ($^{a}p=0.001$, sham vs. hovxe), hsham ($^{b}p=0.004$, hsham vs. hovxe) and hvox ($^{c}p=0.001$, hovx vs. hovxe) (Fig. 7B). In regards to ppar-γ gene expression, it was decreased only in hovxe group, compared to sham ($^{a}p=0.035$) (Fig. 8A). However, significant changes in the Ppar-γ protein levels were observed throughout all groups. Namely, hyperoxia significantly induced Ppar-γ protein level ($^{a}p=0.012$, sham vs. hsham) and E_2 depletion in hyperoxia induced the overexpression of Ppar-γ even more ($^{b}p<0.001$, sham vs. hovx). Again, E_2 administration reverted protein level back to hyperoxia-treated sham group ($^{d}p=0.014$, hovx vs. hovxe), but Ppar-γ protein level was still significantly elevated in comparison to sham-operated normoxic females ($^{c}p=0.016$, sham vs. hovxe (Fig. 8B).

3.8. The effect of E_2 on Ho-1 expression

Further, we have analyzed the expression of Ho-1 to check if hyperoxia alone, or in combination with E_2 manipulation, induced alteration in the expression pattern of yet another protective enzyme. We have observed significant induction of ho-1 gene expression upon hyperoxia treatment in all groups and it was not influenced by either depletion or administration of E_2 (Fig. 9A, $^{abc}p<0.01$ sham vs. hsham, hovx and hovxe). Moreover, the induction of ho-1 gene expression was followed by increased protein level, with similar profile in all treated groups of animals (Fig. 9B, $^{abc}p<0.001$, sham vs. hsham, hovx and hovxe).

3.9. The effect of E_2 on histopathological damage

Histopathological analysis revealed that hyperoxia did not cause any particular changes in liver of any group of mice (Fig. 10, A–D). The number of samples was $n=2$ per each group.

4. Discussion

In this study we have investigated the effect of E_2 against hyperoxia-induced acute oxidative stress in liver of 4 months old

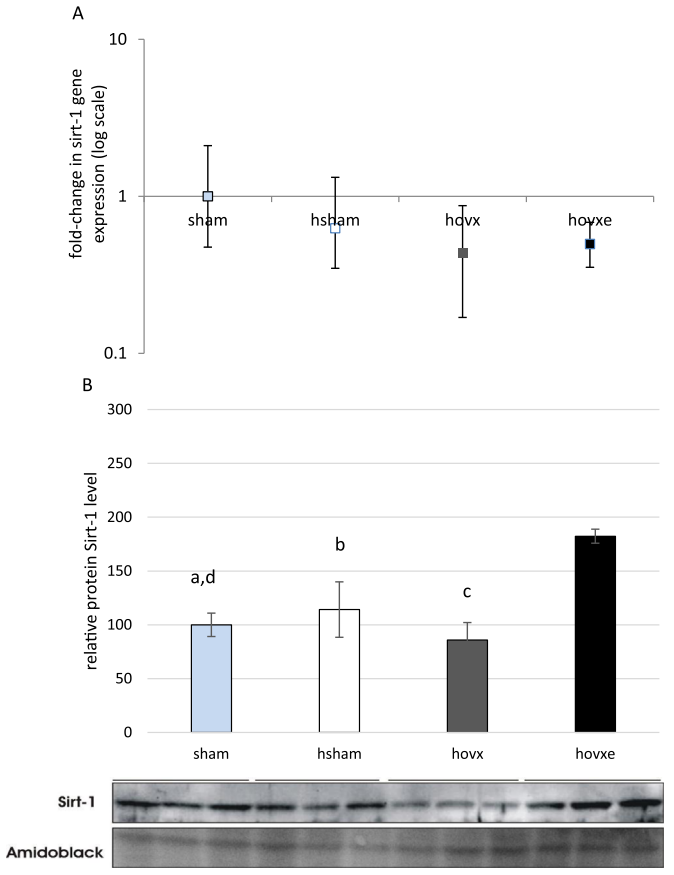

Fig. 7. Real-time PCR analysis of sirt-1 gene expression in the liver of female CBA/H mice subjected to hyperoxia. The fold change in gene expression was calculated using the $2^{-\Delta\Delta CT}$ method and β-actin as the endogenous control. The results are presented as fold-change ± S.E. and normalized to sham group. The number of samples was $n=3$ per each group (A). Western blot analysis of Sirt-1 protein level in the liver of female CBA/H mice subjected to hyperoxia. Results are presented as mean ± S.D. and normalized to sham group. Amidoblack was used as a loading control. The number of samples was $n=3$ per each group. Small letters denote p values. [a]$p=0.001$, sham vs. hovxe; [d]$p=0.035$, sham vs. hovx; [b]$p=0.004$ hsham vs. hovxe; [c]$p=0.001$, hovx vs. hovxe) (B).

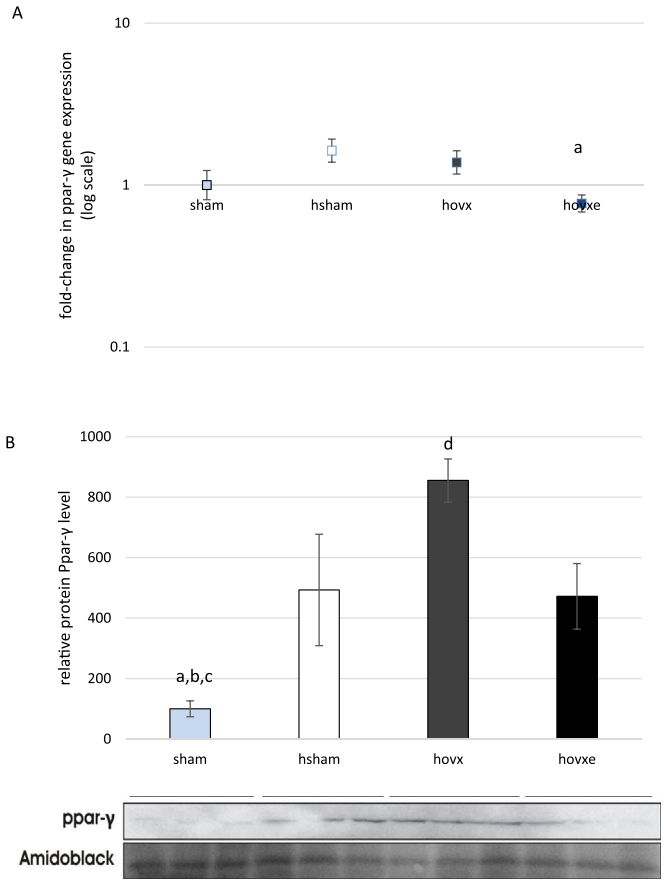

Fig. 8. Real-time PCR analysis of ppar-γ gene expression in the liver of female CBA/H mice subjected to hyperoxia. The fold change in gene expression was calculated using the $2^{-\Delta\Delta CT}$ method and β-actin as the endogenous control. The results are presented as fold-change ± S.E. and normalized to sham group. The number of samples was $n=3$ per each group. Small letter denotes p-value. [a]$p=0.035$, sham vs. hovxe (A). Western blot analysis of Ppar-γ protein level in the liver of female CBA/H mice subjected to hyperoxia. Results are presented as mean ± S.D. and normalized to sham group. Amidoblack was used as a loading control. The number of samples was $n=3$ per each group. Small letters denote p values. [a]$p=0.012$, sham vs. hsham; [b]$p<0.001$, sham vs. hovx; [c]$p=0.016$, sham vs. hovxe; [d]$p=0.014$, hovx vs. hovxe (B).

female CBA/H mice through expression profiling of DPP III, the member of Nrf-2/Keap-1 cytoprotective pathway, and the proteins involved in the cellular response towards oxidative stress, such as Sirt-1, Ppar-γ and Ho-1. Also, to address the question if the E_2-induced reduction of oxidative damage was achieved via upregulation of Nrf-2/Keap-1 signaling pathway,we have determined the nuclear level of Nrf-2 and Keap-1 proteins.

Here we show that hyperoxia alone failed to increase hepatic LPO and decreased DNA damage in sham-operated females. This may be explained by E_2-induced protective response to acute oxidative stress via ERK activation and stimulation of DNA damage repair [26]. Also, the absence of oxidative damage parameters was in parallel with marked accumulation of both DPP III and Nrf-2 proteins in nuclear fractions. Considering Nrf-2, our data suggest the successful attempt of cellular protection against oxidative damage in intact females. This is in accordance with the results of numerous studies which found that the activation of Nrf-2/Keap-1 pathway, i.e. nuclear accumulation of Nrf-2, is protective following oxidative damage (reviewed in [27,28]).

Regarding the upregulation of DPP III expression induced by oxidative stress, we here provide first evidence that DPP III partly translocates from the cytosol into the nucleus of liver cells after in vivo exposure to hyperoxia. In addition, nuclear accumulation of DPP III was even more pronounced in hyperoxia-exposed ovariectomized females treated with E_2. Mechanism responsible for the nuclear targeting of DPP III, i.e. its nuclear localization signal (NLS) is not known. NLSs have diverse patterns of which only a limited number is covered by currently known NLS motifs [29]. However, findings presented in our paper suggest important role of E_2 in the translocation of DPP III to the nucleus upon acute stress conditions. Mouse DPP III (738 amino acid long protein; UniProt entry Q99KK7) contains seven cysteine residues in the molecule, the same number and positions as in the rat enzyme. We have shown earlier that rat DPP III have hyper-reactive sulfhydryl groups [9]. Only recently, it has been reported for a number of proteins that oxidative stress induces nuclear accumulation, or shuttling between subcellular components, via oxidation of cysteine residues (e.g. SECIS binding protein 2 [30] and thioredoxin-interacting protein [31]). Therefore, although nuclear localization signal of mouse DPP III cannot be predicted with high score, having in mind oxidation prone cysteinyl SH-groups in rodent DPP III and unconventional pattern of redox-sensitive NLSs [32], we may consider the possibility that nuclear translocation of mouse DPP III could be regulated by the oxidation state of its cysteine residues. We have recently demonstrated that E_2 depletion in normoxic, physiological conditions caused the increase of endogenous oxidative stress, which can be abolished with E_2 administration [22]. Also, lower oxidative stress in E_2-treated mice was in correlation with increased DPP III protein level, and

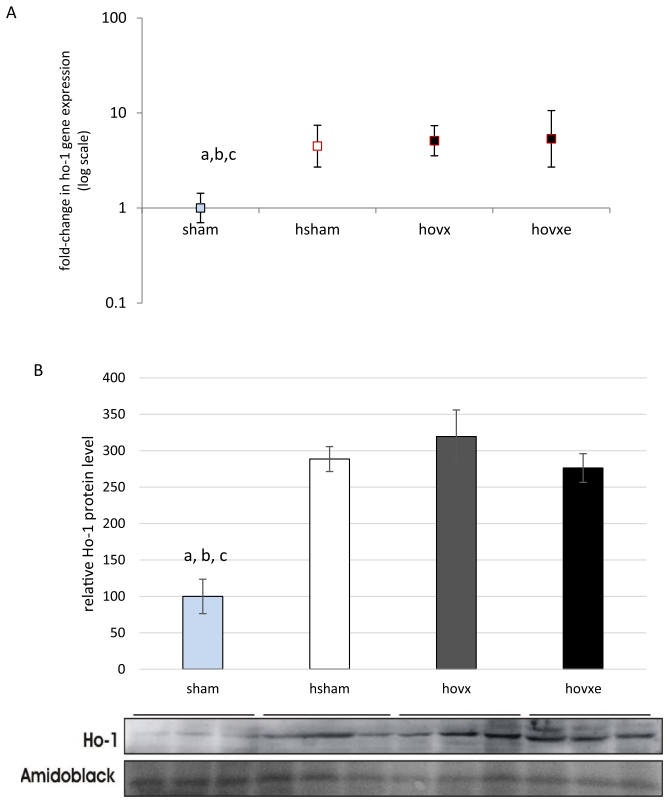

Fig. 9. Real-time PCR analysis of ho-1 gene expression in the liver of female CBA/H mice subjected to hyperoxia. The fold change in gene expression was calculated using the $2^{-\Delta\Delta CT}$ method and β-actin as the endogenous control. The results are presented as fold-change ± S.E. and normalized to sham group. The number of samples was $n=3$ per each group. Small letters denote p values. $^{a,b,c}p<0.01$; sham vs. hsham, hovx and hovxe (A). Western blot analysis of Ho-1 protein level in the liver of female CBA/H mice subjected to hyperoxia. Results are presented as mean ± S.D. and normalized to sham group. Amidoblack was used as a loading control. The number of samples was $n=3$ per each group. Small letters denote p values. $^{abc}p<0.001$, sham vs. hsham, hovx and hovxe (B).

upregulated Ho-1 gene and protein [22]. Moreover, it was reported earlier that significantly lower amount of DPP III protein was found in highly oxygenated rat tissue [9]. In our present study, E_2 depletion under hyperoxic conditions increased LPO and DNA damage, upregulated both Ppar-γ and Ho-1 proteins, all markers of the presence of the oxidative stress. Furthermore, DPP III gene and cytosolic protein expressions were markedly lowered, and E_2 administration reversed both mRNA and protein levels back to those found in normoxic sham group. Considering the major cellular antioxidant GSH, it is interesting to notice that, while in sham-operated mice treated with hyperoxia, GSSG level was only slightly increased, E_2 depletion caused major increment in oxidized form, which was in correlation with the highest level of LPO and lowest cytosolic DPP III protein level in this group. A significant drop in GSSG and restoration of cytosolic DPP III protein content was achieved by subsequent administration of E_2. The inverse relationship between GSSG and Dpp III level found in this study emphasizes previous finding which showed that GSSG is an inactivator of DPP III [33]. Oxidation of cysteine residues might also have an effect on lowering enzymatic activity of DPP III that has remained the same in all groups despite the higher amounts of the protein in hovxe group compared to hovx, and to a lesser extent between hsham and sham group. Taken together, these results contribute towards protective role of E_2 against damage induced by hyperoxia and indicate DPP III as another reliable marker of oxidative stress. However, it is probable that in females other defense strategies against oxidative stress are established, beside GSH pool, for example, increased expression of heme oxygenase that could effectively respond to inducers of oxidative stress [34]. Thus, the importance of GSH system relative to other components of the protective machinery must be taken into account. It has already been shown that enzymatic activity of human DPP III is not required for Keap-1 binding, and subsequent Nrf-2-dependent transcriptional activation, since enzymatically inactive mutant Y318F bound Keap1, and had similar effect on Nrf2-dependent transcription as well as the wild type DPP III [8].

In this study we have shown that E_2 administration exerted protective effect by lowering both LPO and GSSG and through enhancement of DPP III protein level in the cytosol, and its nuclear accumulation. This was accompanied with the upregulation of other cytoprotective enzymes such as Sirt1 and Ho-1, and at the same time, the repression of Ppar-γ, which plays dominant role in adipogenesis, and is also a Sirt-1 target, as shown in [35]. Also, E_2 diminished the accumulation of Nrf-2 in nuclear fraction. The possible reason for the observed repression of Nrf-2/Keap-1 signaling pathway in hyperoxic state induced by E_2, may be that E_2 is able to maintain low level of free radicals via maintenance of mitochondrial function during stress [36], thus reducing the need for cellular defense.

Our results show that downregulation of Sirt-1 protein expression in hovx mice (Fig. 6) corresponds with higher susceptibility to oxidative stress seen as elevated LPO level in the same group (Fig. 1). Sirt-1 is involved in the regulation of stress response, aging and metabolism and its activation is important in suppression of age-related diseases, such as type 2 diabetes, dementia and cardiovascular diseases. Also, Sirt-1 acts as a repressor of adipogenesis [37]. Ovariectomized mice are heavier and have more fat, which is in accordance with the downregulated Sirt-1 and increased level of Ppar-γ protein, the crucial factor in adipogenesis and lipid homeostasis. On the other hand, a significant drop in the body mass was observed in females administered with E_2, compared to their ovariectomized counterparts. This indicates that E_2 might have an inhibitory role on the process of adipogenesis by repressing Ppar-γ, which is in agreement with other studies [38]. Elbaz et al. have also shown the association of E_2 depletion with repression of Sirt-1 and elevated levels of Ppar-γ [39]. Similarly, it has been reported earlier that genotoxic stress or nutrient overload activate Ppar-γ, which binds to Ppar-γ responsive elements in Sirt-1 promoter to repress Sirt-1 expression [40]. Picard et al. [19] also showed that Sirt-1-downregulated cells had higher levels of Ppar-γ and vice versa. Also, Sirt-1 is shown to be increased during fasting or in long-lived animals and decreased in conditions of obesity and insulin resistance [41]. Besides, Sirt-1 exerts anti-inflammatory effects [42]. Induction of Sirt-1 has been proposed as a therapeutic target in treatment of several metabolic and age-related diseases. On the other hand, Ppar-γ activation in mice models for insulin resistant diabetes has been shown to be beneficial [43]. These contradictory results require more investigation, and other factors, such as cofactors, transcription factors and signaling molecules from numerous pathways must be taken into account.

5. Conclusions

Here we show that in adult female CBA/H mice subjected to hyperoxia and depleted of E_2, both DPP III gene and cytosolic protein expression were lowered, along with Sirt-1 expression, which was followed with highest level of oxidative stress. Subsequent E_2 administration reversed both DPP III and Sirt-1 levels back to levels measured in control group, resulting in reduction of oxidative damage. DPP III accumulated in the nucleus in response to hyperoxia, while combination of hyperoxia and E_2

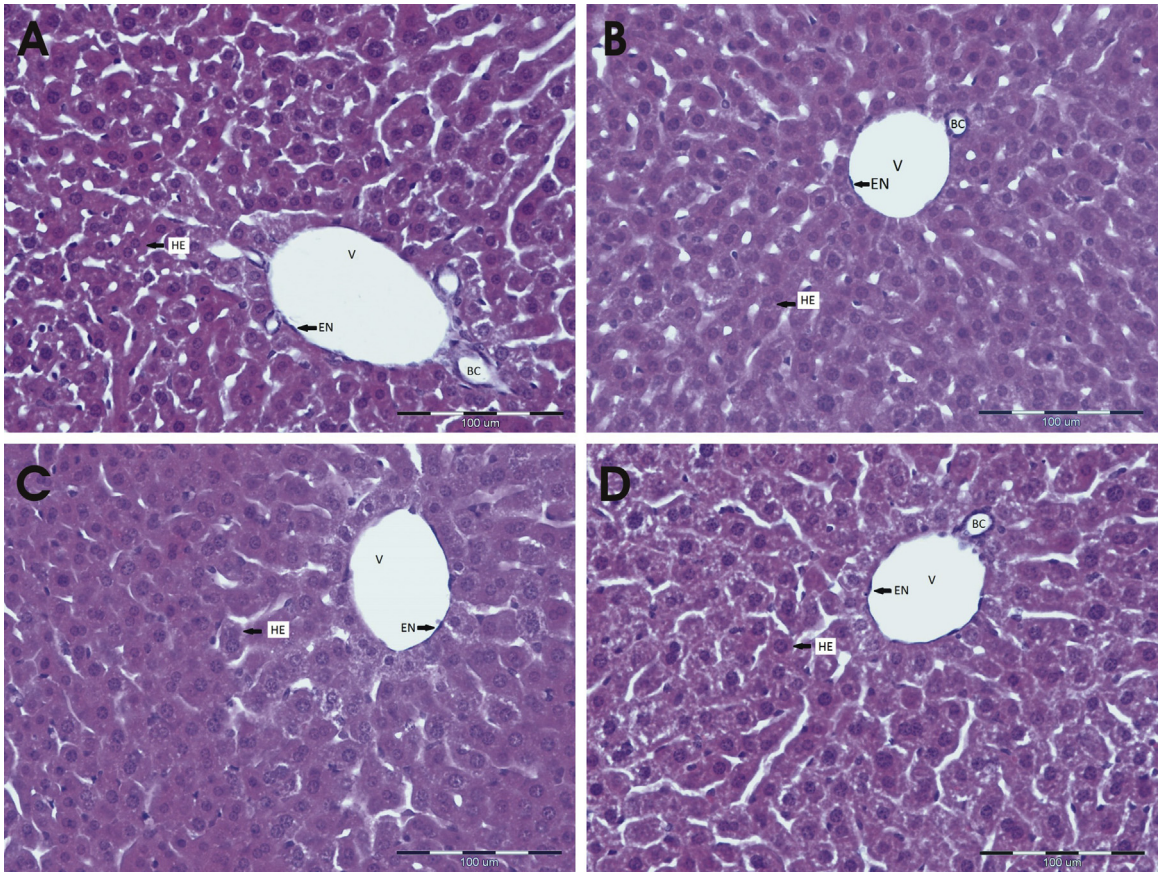

Fig. 10. Histopathological findings in liver of hyperoxia-treated female mice. Compared to sham-operated normoxic females (A), hyperoxia did not cause any particular changes in liver of hyperoxia-treated sham-operated females (B) nor in hyperoxia-treated ovariectomized females without (C) and with E_2 (D). The number of samples was $n=2$ per each group. Abbreviations denote as follows; HE, hepatocytes; V, vein; EN, endothelial cells; BC, bile canaliculus.

administration displayed the cumulative effect on DPP III translocation to the nucleus. Although DPP III has so far been considered as a cytosolic protein, our study reveal nuclear localization in mice liver cells, suggesting that DPP III may shuttle within the cell.

Moreover, the extent of the nuclear accumulation of Nrf-2, a known regulator of antioxidative defense, was comparable with increased nuclear level of DPP III, when healthy female mice were exposed to hyperoxia. This suggests that DPP III could participate in Nrf-2-induced adaptive response triggered by oxidative stress. In the presence of E_2, Sirt-1 and DPP III proteins markedly increased, unlike Nrf-2. In addition, results of this study lead us to propose that in young, adult, healthy females, E_2 exhibits protective effect towards the oxidative stress via upregulation of DPP III, Ho-1, Sirt-1, decrease in GSSG and suppression of Ppar-γ. This finding suggests the role of DPP III along with Sirt-1 in E_2-mediated protection against hyperoxia. However, the presence of other cytoprotective strategies cannot be neglected. These data may contribute to better understanding of relationship between E_2, DPP III and Nrf-2/Keap-1 axis and females' resistance to oxidative stress. Besides, distinguishing the pathways involved in beneficial and detrimental effects of E_2 is crucial for developing drug therapies that will help retard aging with only minimal deleterious effects caused by E_2.

Declaration of interest statement

No conflicts of interest declared.

Author contribution

Sandra Sobočanec and Vedrana Filić contributed equally to this work.

Acknowledgments

The authors would like to thank Iva Pešun Međimorec for her excellent technical contribution in performing surgical procedures of ovariectomy and Ana Jagust for her excellent technical assistance in performing immunohistochemical analyses. The authors want to thank Dr. Anita Kriško and Dr. Igor Weber for critical evaluation of the Manuscript. This research is funded by Croatian Ministry of Science, Education and Sports, Grant nos. 098-0982464-1647, 098-1191344-2938, IBRO 2013 RHP and FP7-REG-POT-2012-2013-1, Grant agreement number 316289 – InnoMol.

Appendix A. Supplementary material

Supplementary data associated with this article can be found in the online version at http://dx.doi.org/10.1016/j.redox.2016.01.003.

References

[1] H.R. Potteti, N.M. Reddy, T.K. Hei, D.V. Kalvakolanu, S.P. Reddy, The NRF2 activation and antioxidative response are not impaired overall during hyperoxia-induced lung epithelial cell death, Oxidative Med. Cell. Longev. 2013 (2013)

798401, http://dx.doi.org/10.1155/2013/798401.
[2] G.N. Landis, D. Abdueva, D. Skvortsov, J. Yang, B.E. Rabin, et al., Similar gene expression patterns characterize aging and oxidative stress in *Drosophila melanogaster*, Proc. Natl. Acad. Sci. USA 101 (2004) 7663–7668.
[3] P. Kapahi, M.E. Boulton, T.B. Kirkwood, Positive correlation between mammalian life span and cellular resistance to stress, Free Radic. Biol. Med. 26 (1999) 495–500.
[4] S.C. Manolagas, From estrogen-centric to aging and oxidative stress: a revised perspective of the pathogenesis of osteoporosis, Endocr. Rev. 31 (2010) 266–300, http://dx.doi.org/10.1210/er.2009-0024.
[5] A. Šaric, S. Sobočanec, Z.M. Safranko, M. Popovic-Hadzija, G. Aralica, et al., Female headstart in resistance to hyperoxia-induced oxidative stress in mice, Acta Biochim. Pol. 61 (2014) 801–807.
[6] M. Abramic, M. Zubanovic, L. Vitale, Dipeptidyl peptidase III from human erythrocytes, Biol. Chem. Hoppe Seyler 369 (1988) 29–38.
[7] Y. Liu, J.T. Kern, J.R. Walker, J.A. Johnson, P.G. Schultz, et al., A genomic screen for activators of the antioxidant response element, Proc. Natl. Acad. Sci. USA 104 (2007) 5205–5210, http://dx.doi.org/10.1073/pnas.0700898104.
[8] B.E. Hast, D. Goldfarb, K.M. Mulvaney, M.A. Hast, P.F. Siesser, et al., Proteomic analysis of ubiquitin ligase KEAP1 reveals associated proteins that inhibit NRF2 ubiquitination, Cancer Res. 73 (2013) 2199–2210, http://dx.doi.org/10.1158/0008-5472.CAN-12-4400.
[9] M. Abramic, S. Simaga, M. Osmak, L. Cicin-Sain, B. Vukelic, et al., Highly reactive cysteine residues are part of the substrate binding site of mammalian dipeptidyl peptidases III, Int. J. Biochem. Cell Biol. 36 (2004) 434–446.
[10] N. Li, M.I. Venkatesan, A. Miguel, R. Kaplan, C. Gujuluva, et al., Induction of heme oxygenase-1 expression in macrophages by diesel exhaust particle chemicals and quinones via the antioxidant-responsive element, J. Immunol. 165 (2000) 3393–3401.
[11] M. McMahon, K. Itoh, M. Yamamoto, J.D. Hayes, Keap1-dependent proteasomal degradation of transcription factor Nrf2 contributes to the negative regulation of antioxidant response element-driven gene expression, J. Biol. Chem. 278 (2003) 21592–21600, http://dx.doi.org/10.1074/jbc.M300931200.
[12] L.G. Higgins, M.O. Kelleher, I.M. Eggleston, K. Itoh, M. Yamamoto, et al., Transcription factor Nrf2 mediates an adaptive response to sulforaphane that protects fibroblasts in vitro against the cytotoxic effects of electrophiles, peroxides and redox-cycling agents, Toxicol. Appl. Pharmacol. 237 (2009) 267–280, http://dx.doi.org/10.1016/j.taap.2009.03.005.
[13] H.Y. Cho, S.P. Reddy, A. Debiase, M. Yamamoto, S.R. Kleeberger, Gene expression profiling of NRF2-mediated protection against oxidative injury, Free Radic. Biol. Med. 38 (2005) 325–343, http://dx.doi.org/10.1016/j.freeradbiomed.2004.10.013.
[14] S.M. Rangwala, M.A. Lazar, Peroxisome proliferator-activated receptor gamma in diabetes and metabolism, Trends Pharmacol. Sci. 25 (2004) 331–336.
[15] H.Y. Cho, W. Gladwell, X. Wang, B. Chorley, D. Bell, et al., Nrf2-regulated PPAR {gamma} expression is critical to protection against acute lung injury in mice, Am. J. Respir. Crit. Care Med. 182 (2010) 170–182, http://dx.doi.org/10.1164/rccm.200907-1047OC.
[16] U.A. Boelsterli, M. Bedoucha, Toxicological consequences of altered peroxisome proliferator-activated receptor gamma (PPARgamma) expression in the liver: insights from models of obesity and type 2 diabetes, Biochem. Pharmacol. 63 (2002) 1–10, http://dx.doi.org/10.1016/S0006-2952(01)00817-6.
[17] H. Yamamoto, K. Schoonjans, J. Auwerx, Sirtuin functions in health and disease, Mol. Endocrinol. 21 (2007) 1745–1755, http://dx.doi.org/10.1210/me.2007-0079.
[18] H.L. Cheng, R. Mostoslavsky, S. Saito, J.P. Manis, Y. Gu, et al., Developmental defects and p53 hyperacetylation in Sir2 homolog (SIRT1)-deficient mice, Proc. Natl. Acad. Sci. USA 100 (2003) 10794–10799, http://dx.doi.org/10.1073/pnas.1934713100.
[19] F. Picard, M. Kurtev, N. Chung, A. Topark-Ngarm, T. Senawong, et al., Sirt1 promotes fat mobilization in white adipocytes by repressing PPAR-gamma, Nature 429 (2004) 771–776, http://dx.doi.org/10.1038/nature02583.
[20] H. Ohkawa, N. Ohishi, K. Yagi, Assay for lipid peroxides in animal tissues by thiobarbituric acid reaction, Anal. Biochem. 95 (1979) 351–358.
[21] R.R. Tice, E. Agurell, D. Anderson, B. Burlinson, A. Hartmann, et al., Single cell gel/comet assay: guidelines for in vitro and in vivo genetic toxicology testing, Environ. Mol. Mutagen. 35 (2000) 206–221.
[22] Ž. Mačak Šafranko, S. Sobočanec, A. Šarić, N. Jajčanin-Jozić, Ž. Krsnik, et al., The effect of 17beta-estradiol on the expression of dipeptidyl peptidase III and heme oxygenase 1 in liver of CBA/H mice, J. Endocrinol. Investig. 38 (2015) 471–479.
[23] A.A. Stillman, Z. Krsnik, J. Sun, M.R. Rasin, M.W. State, et al., Developmentally regulated and evolutionarily conserved expression of SLITRK1 in brain circuits implicated in Tourette syndrome, J. Comp. Neurol. 513 (2009) 21–37, http://dx.doi.org/10.1002/cne.21919.
[24] S. Sobocanec, A. Saric, Z. Macak Safranko, M. Popovic Hadzija, M. Abramic, et al., The role of 17beta-estradiol in the regulation of antioxidant enzymes via the Nrf2–Keap1 pathway in the livers of CBA/H mice, Life Sci. 130 (2015) 57–65, http://dx.doi.org/10.1016/j.lfs.2015.03.014.
[25] H. Williams, P.A. Dacks, N.E. Rance, An improved method for recording tail skin temperature in the rat reveals changes during the estrous cycle and effects of ovarian steroids, Endocrinology 151 (2010) 5389–5394, http://dx.doi.org/10.1210/en.2010-0630.
[26] A. Porzionato, M.M. Sfriso, A. Mazzatenta, V. Macchi, R. De Caro, et al., Effects of hyperoxic exposure on signal transduction pathways in the lung, Respir. Physiol. Neurobiol. 209 (2015) 106–114, http://dx.doi.org/10.1016/j.resp.2014.12.002.
[27] D.D. Zhang, Mechanistic studies of the Nrf2–Keap1 signaling pathway, Drug Metab. Rev. 38 (2006) 769–789.
[28] T.M. Stepkowski, M.K. Kruszewski, Molecular cross-talk between the NRF2/KEAP1 signaling pathway, autophagy, and apoptosis, Free Radic. Biol. Med. 50 (2011) 1186–1195, http://dx.doi.org/10.1016/j.freeradbiomed.2011.01.033.
[29] J.R. Lin, J. Hu, SeqNLS: nuclear localization signal prediction based on frequent pattern mining and linear motif scoring, PLoS One 8 (2013) e76864, http://dx.doi.org/10.1371/journal.pone.0076864.
[30] L.V. Papp, J. Lu, F. Striebel, D. Kennedy, A. Holmgren, et al., The redox state of SECIS binding protein 2 controls its localization and selenocysteine incorporation function, Mol. Cell. Biol. 26 (2006) 4895–4910, http://dx.doi.org/10.1128/MCB.02284-05.
[31] G. Saxena, J. Chen, A. Shalev, Intracellular shuttling and mitochondrial function of thioredoxin-interacting protein, J. Biol. Chem. 285 (2010) 3997–4005, http://dx.doi.org/10.1074/jbc.M109.034421.
[32] S. Kosugi, M. Hasebe, N. Matsumura, H. Takashima, E. Miyamoto-Sato, et al., Six classes of nuclear localization signals specific to different binding grooves of importin alpha, J. Biol. Chem. 284 (2009) 478–485, http://dx.doi.org/10.1074/jbc.M807017200.
[33] Z. Karacic, J. Spoljaric, M. Rozman, M. Abramic, Molecular determinants of human dipeptidyl peptidase III sensitivity to thiol modifying reagents, Biol. Chem. 393 (2012) 1523–1532, http://dx.doi.org/10.1515/hsz-2012-0181.
[34] S. Dore, M. Takahashi, C.D. Ferris, R. Zakhary, L.D. Hester, et al., Bilirubin, formed by activation of heme oxygenase-2, protects neurons against oxidative stress injury, Proc. Natl. Acad. Sci. USA 96 (1999) 2445–2450.
[35] G.E. Simmons Jr., W.M. Pruitt, K. Pruitt, Diverse roles of SIRT1 in cancer biology and lipid metabolism, Int. J. Mol. Sci. 16 (2015) 950–965, http://dx.doi.org/10.3390/ijms16010950.
[36] J.W. Simpkins, K.D. Yi, S.H. Yang, Role of protein phosphatases and mitochondria in the neuroprotective effects of estrogens, Front. Neuroendocr. 30 (2009) 93–105, http://dx.doi.org/10.1016/j.yfrne.2009.04.013.
[37] E.D. Rosen, O.A. MacDougald, Adipocyte differentiation from the inside out, Nat. Rev. Mol. Cell Biol. 7 (2006) 885–896, http://dx.doi.org/10.1038/nrm2066.
[38] A. Foryst-Ludwig, M. Clemenz, S. Hohmann, M. Hartge, C. Sprang, et al., Metabolic actions of estrogen receptor beta (ERbeta) are mediated by a negative cross-talk with PPARgamma, PLoS Genet. 4 (2008) e1000108, http://dx.doi.org/10.1371/journal.pgen.1000108.
[39] A. Elbaz, D. Rivas, G. Duque, Effect of estrogens on bone marrow adipogenesis and Sirt1 in aging C57BL/6J mice, Biogerontology 10 (2009) 747–755.
[40] B.J. Morris, Seven sirtuins for seven deadly diseases of aging, Free Radic. Biol. Med. 56 (2013) 133–171, http://dx.doi.org/10.1016/j.freeradbiomed.2012.10.525.
[41] M.C. Haigis, D.A. Sinclair, Mammalian sirtuins: biological insights and disease relevance, Annu. Rev. Pathol. 5 (2010) 253–295, http://dx.doi.org/10.1146/annurev.pathol.4.110807.092250.
[42] M.P. Gillum, M.E. Kotas, D.M. Erion, R. Kursawe, P. Chatterjee, et al., SirT1 regulates adipose tissue inflammation, Diabetes 60 (2011) 3235–3245, http://dx.doi.org/10.2337/db11-0616.
[43] B.M. Spiegelman, PPAR-gamma: adipogenic regulator and thiazolidinedione receptor, Diabetes 47 (1998) 507–514.